Organic & Biomolecular Chemistry

RSC Publishing

PAPER

View Article Online
View Journal | View Issue

Cite this: *Org. Biomol. Chem.*, 2013, **11**, 4397

Hybrid photoactive fullerene derivative–ruboxyl nanostructures for photodynamic therapy†

Alexander I. Kotelnikov,*[a] Alexander Yu. Rybkin,[a] Ekaterina A. Khakina,[a] Alexey B. Kornev,[a] Alexander V. Barinov,[a] Nikolay S. Goryachev,[a] Anastasiya V. Ivanchikhina,[a] Alexander S. Peregudov,[b] Vyacheslav M. Martynenko[a] and Pavel A. Troshin*[a]

Received 22nd January 2013,
Accepted 5th April 2013

DOI: 10.1039/c3ob40136g

www.rsc.org/obc

Here we report the investigation of photophysical properties and photodynamic action of two novel water soluble hybrid molecular structures based on [60]fullerene dyads bearing covalently attached residues of anthracycline antibiotic "ruboxyl". Molecular structures of the designed compounds were confirmed by IR and UV-VIS absorption spectroscopy, electrospray mass spectrometry (compound **5**), and ^{1}H and ^{13}C NMR spectroscopy. Dynamic light scattering, steady-state and kinetic fluorimetry and UV-VIS absorption spectroscopy techniques were used to study the behavior of the synthesized hybrid molecular structures in aqueous solutions. Photodynamic activity of the compounds was evaluated by monitoring the O_2^- generation under visible light irradiation using the NBT test. It has been shown that the anthracycline chromophore (ruboxyl moiety possesses no photodynamic activity) behaves as an efficient photosensitizer for the fullerene core operating *via* the energy and/or the electron transfer pathways. The presented approach opens up wide opportunities for the design of various fullerene-based donor–acceptor systems with enhanced photodynamic properties potentially suitable for biomedicinal applications.

1. Introduction

It is known that [60]fullerene exhibits exciting photophysical and electronic properties due to its unique three-dimensional structure. Pristine fullerene and its derivatives are efficient electron donors in the photoexcited state and rather strong electron acceptors in the ground state. They generate efficiently singlet oxygen $^{1}O_2$ under light excitation.[1] Fullerene-based systems also generate superoxide radical anion $O_2^{\cdot -}$ and other active oxygen species under visible light illumination in the presence of molecular oxygen and electron donors.[2] Recently, many papers have been published on a photodynamic effect of fullerenes and their derivatives resulting in the damage of DNA, proteins and membranes, as well as a suppression of tumor cells, viruses and bacteria growth.[3–14] Unfortunately, the application of fullerenes and their derivatives for photodynamic therapy in clinical practice is strongly limited by a weak absorption of fullerenes at long wavelengths in the visible (VIS) and near infrared (NIR) spectral ranges. The short wavelength absorptions characteristic for fullerenes are hardly suitable for a photodynamic therapy since such beams do not penetrate deep into living tissues. The efficiency of the photodynamic action of fullerenes can be greatly enhanced by using hybrid nanostructures (HNS) composed of fullerene derivatives bearing appended dye molecules absorbing the light in the VIS and NIR spectral ranges.

It is known that [60]fullerene has a singlet excited energy state at 16 000 cm^{-1} and a triplet excited state at 12 700 cm^{-1}.[1] The absorption of a photon by a dye–fullerene conjugate might lead to many different events. For instance, the excitation energy can be potentially transferred from the dye molecule to the fullerene cage or *vice versa* depending on the frontier energy levels of these subunits. Moreover, the energy transfer to an intermediate charge transfer state (CT state) also becomes possible if such a CT state is formed in the system. In addition, a photoinduced electron transfer can occur from the photoexcited dye block thus producing a charge separated state (CS state). Alternatively, the CS state can be produced *via* electron abstraction by the excited fullerene unit from the dye unit in the ground state. The formation of the excited fullerene states or the fullerene radical anion in biological systems initiates a cascade of chemical reactions producing active molecular and radical species. The singlet oxygen $^{1}O_2$ and oxygen radical anion $O_2^{\cdot -}$ formed *via* quenching of the fullerene excited state or a fullerene radical anion by molecular O_2

[a]*IPCP RAS, Semenov Prospect 1, Chernogolovka, 141432, Russia. E-mail: kotel@icp.ac.ru, troshin@icp.ac.ru; Fax: +7 496522-3507; Tel: +7 496522 1418*
[b]*INEOS RAS, Vavylova St. 28, B-334, Moscow, 119991, Russia*

†Electronic supplementary information (ESI) available: FT-IR spectra of compounds **1**, **3** and **4**. See DOI: 10.1039/c3ob40136g

are the most common examples. A reduction of the dye radical cation or an oxidation of the fullerene radical anion by different compounds persisting in living tissues (for instance, such reductants as NADH, cysteine, ascorbic acid) might complicate the reaction pathways. Nevertheless, the neat effect of such processes is the formation of some active species under the light excitation inducing local destruction of the tissue. The design of HNS with optimized structural, photophysical and redox parameters is a big challenge in the field of photodynamic therapy.

Many fullerene-based photoactive donor–acceptor dyads and triads have been synthesized recently for application in solar energy conversion devices.[15–20] However, these systems are hardly suitable for photodynamic therapy primarily because they lack solubility in water or biological media and the ability for selective accumulation in the therapeutic targets such as tumor cells. There are very few publications reporting the synthesis of HNS based on covalent conjugates of fullerene derivatives with dye molecules (*e.g.* acridine or porphyrin dyes) and the investigation of their photodynamic action in biological systems.[21–24] The vast majority of these HNS are weakly soluble in water which complicates their administration to living tissues and, most importantly, subsequent excretion from the organism.

Here we report the synthesis and investigation of highly water-soluble fullerene-based HNS comprising photoactive ruboxyl units (an anthracycline antibiotic similar to daunorubicin and doxorubicin[25]) attached to water soluble fullerene C_{60} derivatives.

2. Experimental

2.1. General

NADH (nicotinamide adenine dinucleotide, Sigma), NBT (nitro blue tetrazolium chloride, MP Biomedical, Germany), EDTA (ethylenediaminetetraacetic acid, Sigma), $Na_2HPO_4{\cdot}6H_2O$ and $NaH_2PO_4{\cdot}H_2O$ (MP Biomedicals, Germany) were used.

Absorption spectra were recorded using a Specord M-40 spectrophotometer equipped with a computer interface and a temperature-controlled sample unit. Fluorescence spectra were measured using a Cary-Eclipse spectrofluorimeter. Kinetics of fluorescence decays were recorded by "Fluo Time 200" PicoQuant GmbH.

2.2. Photochemical and photophysical studies

Photochemical activity of the compounds (relative amount of the superoxide radicals produced) was investigated using a standard formazan assay by measuring the evolution of the optical density at 560 nm.[2] Photochemical reactions were performed in a 1 × 1 cm quartz cuvette illuminated inside a temperature-controlled sample unit stabilized at 20 °C. The cuvette was filled with 2 mL of phosphate buffer solution (pH = 6.5, 0.05 M). NADH (4×10^{-4} M), NBT (4.8×10^{-5} M), EDTA (2×10^{-5} M) and then compounds **1–5** (Fig. 1) were added to achieve a concentration of 10^{-5} M. Photodynamic properties of

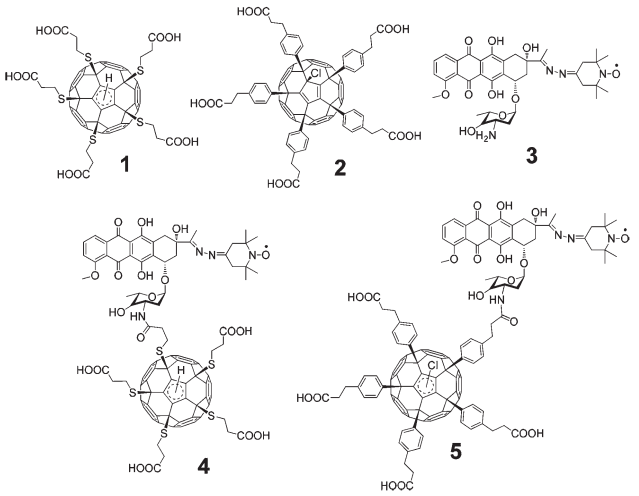

Fig. 1 Molecular structures of compounds **1–5**.

1–5 were investigated using the illumination provided by a high pressure xenon lamp (150 W) passed through a system of optical filters selecting the 490–510 nm band (corresponds to the absorption maximum of ruboxyl) and cutting off the shorter and longer wavelengths. The power of the light illuminating the sample was ~4.4 mW cm^{-2}. Illumination in the UV range was realized using an alternative system of optical filters with maximal transmission near the 360 nm wavelength and "blind" areas in the visible, NIR and IR ranges. The power of the incident UV light flux was ~8.0 mW cm^{-2}.

2.3. Dynamic light scattering experiments

Aqueous solutions of fullerene derivatives (4 mg mL^{-1}) were filtered through syringe filters and poured into vials that were prewashed several times with filtered water in order to remove dust particles. The solutions were then thermostated for about 2 hours at 20 °C thus allowing the systems to reach an equilibrium. The temperature control accuracy was 0.1 °C. Dynamic light scattering (DLS) measurements were performed at a detection angle of 90° with a Photocor Complex (Photocor Instruments Inc., USA; http://www.photocor.com) setup equipped with a He–Ne laser (λ = 679.5 nm). The mutual diffusion coefficients of fullerene aggregates were computed from the DLS data using the DynaLS program (Alango, Israel). Hydrodynamic diameters of the fullerene aggregates were calculated from the mutual diffusion coefficients using the Einstein–Stokes formula for diffusion coefficients of spherical particles. The viscosity (η = 1.006) and the refractive index (n = 1.33268) of water were used.

2.4. Synthesis of conjugates 4 and 5

Polycarboxylic derivatives of fullerenes **1** and **2** were synthesized according to the previously reported procedures.[26,27] The conjugation of **1** and **2** with ruboxyl **3** has been carried out using a following general procedure. The fullerene derivative **1** or **2** (1.0 eq.) was dissolved in dry THF under gentle magnetic stirring at room temperature (final concentration of

ca. 5–10 mg of **1** or **2** per 1 mL of THF was achieved). A small excess (1.1 eq.) of 1-hydroxybenzotriazole (BtOH) and a catalytic amount (20–30 mg) of 4-dimethylaminopyridine (DMAP) were added to the reaction mixture. These were followed by 1.1 eq. of dicyclohexylcarbodiimide (DCC) dissolved in tetrahydrofuran (4–10 mL) and the mixture was stirred for the next 3 hours while the activated Bt-esters of the corresponding fullerene derivatives were formed. Ruboxyl (1.5 eq.) was dissolved in a THF (2 mL), pyridine (4 mL) and Et_3N (1 mL) mixture and the resulting solution was added to the reaction mixture comprising the activated ester of the fullerene derivative. The mixture was stirred overnight, the formed precipitate of dicyclohexylurea was filtered off, the filtrate was concentrated on a rotary evaporator and the viscous red–brown residue was solidified by the addition of ethyl acetate. The precipitate was separated by centrifugation and dried in air. The compositions and molecular structures of the synthesized compounds **4** and **5** were confirmed by chemical analysis, FT-IR spectroscopy, ^1H and ^{13}C NMR spectroscopy for **4** and also by electrospray mass spectrometry for **5**. Conjugates **4** and **5** were transformed to the water soluble salts by treatment with equivalent amounts of an aqueous solution of potassium carbonate and subsequent freeze drying.

Compound **4**. ^1H NMR (DMSO-D_6, 600 MHz): 1.03 (m, 3H), 1.19 (s, 12H), 1.24 (m, 2H), 1.61 (s, 2H), 1.73 (m, 4H), 2.72 (m, 4H), 2.88 (m, 2H), 3.07 (m, 10 H), 3.39 (m, 18H), 4.02 (m, 5H), 5.62 (s, 1H), 6.87 (s, 1H), 7.39 (m, 1H), 7.89 (m, 1H), 8.18 (m, 1H). ^{13}C NMR (DMSO-D_6, 150 MHz): 9.05, 14.57, 21.26, 24.94, 25.80, 28.37, 33.47, 33.82, 34.06, 35.96, 45.95, 47.96, 57.14, 57.58, 60.25, 107.35, 110.51, 119.26, 124.40, 126.72, 128.17, 136.64, 142.53, 142.90, 143.30, 145.62, 146.34, 146.64, 146.71, 148.24, 150.09, 154.98, 156.53, 157.10, 170.83, 173.14, 173.61. FT-IR (KBr pellet, ν, cm^{-1}): 528 (M), 542 (M), 745 (W), 765 (W), 808 (M), 988 (S), 1016 (S), 1037 (S), 1066 (M), 1081 (M), 1116 (S), 1211 (VS), 1235 (S), 1284 (S), 1379 (S), 1404 (VS), 1443 (S), 1562 (S), 1576 (S), 1617 (S), 1645 (VS), 1728 (S), 2928 (S), 3083 (M), 3422 (S). Chemical analysis: calculated C, 69.33; H, 3.62; N, 2.91; S, 8.34. Found: C, 69.14; H, 3.70; N, 2.73; S, 8.32%.

Compound **5**. FT-IR (KBr pellet, ν, cm^{-1}): 454 (W), 464 (W), 480 (W), 498 (W), 542 (M), 566 (W), 586 (W), 650 (W), 704 (W), 764 (W), 792 (W), 818 (W), 842 (W), 910 (W), 988 (M), 1020 (M), 1040 (M), 1066 (W), 1082 (W), 1114 (W), 1156 (W), 1210 (M), 1236 (M), 1284 (M), 1376 (M), 1412 (M), 1432 (M), 1444 (M), 1462 (M), 1510 (M), 1552 (W), 1582 (M), 1620 (M), 1640 (M), 1678 (W), 1712 (M), 1728 (M), 2934 (M), 2976 (M), 3026 (W), 3432 (VS), 3440 (VS). ESI-MS: calculated *m*/*z* 1087.8 ($[M - 2H]^{2-}$), found 1087.3. Chemical analysis: calculated C, 77.77; H, 4.07; N, 2.57; Cl, 1.63. Found: C, 77.86; H, 4.11; N, 2.47; Cl, 1.48%.

3. Results and discussion

3.1. Synthesis and characterization of 4 and 5

The choice of the ruboxyl **3** as a photosensitizer used for conjugation with the fullerene derivatives was motivated by the following reasons. First of all, ruboxyl is known as a promising anticancer antibiotic demonstrating significantly improved pharmacological properties compared to the similar daunorubicin or doxorubicin analogs.[25] At the same time, ruboxyl exhibits intense absorption (λ_{max} = 470–500 nm) and luminescence (λ_{max} = 590 nm) bands in the visible range and therefore might be considered as a promising candidate for sensitizing the fullerene. The advanced optical properties of ruboxyl allow a detailed spectral analysis of the photochemical reactions of the fullerene–ruboxyl hybrid structures to be performed.

The fullerene derivatives **1** and **2** have superior molecular structure: all five organic addends bearing solubilizing carboxylic groups are attached to one hemisphere of the fullerene molecule around a central pentagon unit thus leaving the rest of the carbon cage available for interactions (particularly, hydrophobic) with different biological targets. We have shown previously that such a molecular structure leads to a pronounced antiviral activity in combination with a low toxicity.[27] Another advantage of compounds **1** and **2** is their exceptionally high (>100 mg mL^{-1}) solubility in water in the form of sodium or potassium salts which makes possible their easy administration to biological systems varying from cell cultures to living animals.

One or more carboxylic groups in the **1** or **2** molecules can be potentially coupled with the ruboxyl units using standard carbodiimide approach (see Experimental). Our previous experience showed that it is necessary to keep 3–4 unmodified carboxylic (or carboxylate COO^-) groups in the molecule of the conjugate to maintain the solubility of the product in water on a reasonable level of 1–10 mg mL^{-1}. Here we intentionally performed the coupling of the fullerene derivatives **1** and **2** with just one ruboxyl molecule per fullerene cage. Scheme 1 illustrates the synthesis of conjugate **5**.

The obtained conjugates **4** and **5** were first characterized by their FT-IR spectra. It was shown that the spectra of conjugates are represented mainly by the superposition of the spectra of individual components except for two major features. First of all, some bands were shifted by 5–10 cm^{-1} compared to the pristine components due to the conjugation effect. Second, an amide bond appeared at 1728 cm^{-1} thus confirming the covalent bonding of ruboxyl to the fullerene derivatives. The IR spectra of the fullerene derivative **1**, ruboxyl **3** and the conjugate **4** are shown in Fig. S1 (see ESI†).

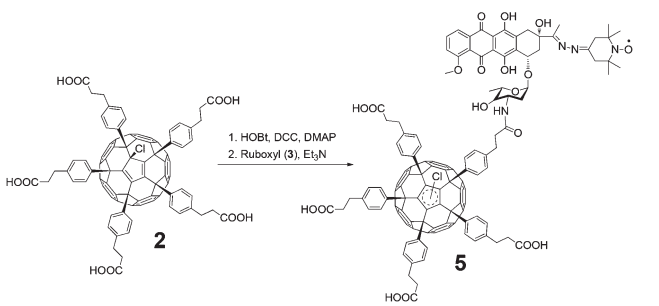

Scheme 1 Preparation of conjugate **5**.

The characterization of conjugates **4** and **5** by NMR spectroscopy was complicated by the presence of a nitroxyl radical unit in their molecular frameworks. It is known that radical species do not give well-resolved NMR spectra. Similar behavior was also observed in the case of **4** and **5** (Fig. S2†). Nevertheless, the ^{1}H NMR spectrum of **4** showed all the signals expected for this complicated molecular architecture. At the same time, the low field ^{13}C NMR spectrum revealed the fullerene cage profile (groups of signals marked with "*") which is characteristic of the C_s-symmetry adduct derived *via* distortion of the C_{5v}-symmetrical structure by modifying one carboxylic group with the ruboxyl unit (and the hydrogen atom trotting around the central cyclopentadienyl unit, see details in ref. 28). The peaks corresponding to the ruboxyl sp^2 carbons were also clearly detectable in the spectrum. The high field ^{13}C NMR exhibited a number of signals corresponding to the sp^3 carbons of the ruboxyl moiety and the fullerene derivative (the latter are marked with "*"). The NMR spectra of compound **5** (Fig. S3†) were somewhat more complicated compared to the similar spectra of compound **4**. In contrast to compound **4** with a hydrogen atom trotting around the central 5-membered ring, the chlorine atom in compound **5** forms a rigid bond with a fullerene cage. This leads to the co-existence of three isomers of compound **5** which differ from each other by the relative positions of Cl and the aryl group loaded with a ruboxyl moiety.

All our attempts to obtain a mass spectrum of compound **4** failed presumably due to the decomposition of this complex molecule under the electrospray ionization (ESI) conditions. On the contrary, the ESI mass spectrum of the more stable conjugate **5** revealed a distinct peak at m/z = 1087.3 corresponding to the $[\mathbf{5\text{-}2H}]^{2-}$ dianion (Fig. S6†).

Thus, all the obtained spectroscopic data conform to the proposed molecular structures of conjugates **4** and **5** shown in Fig. 1. However, it is not clear what kinds of species are formed in the aqueous solutions obtained by dissolving potassium salts of **4** (**4-K**) and **5** (**5-K**) in water. To answer this question we performed a dynamic light scattering (DLS) study of aqueous solutions of **4** and **5** (concentration range 10^{-4}–10^{-3} mol L^{-1}). The DLS experiments revealed the formation of well-organized supramolecular architectures with average hydrodynamic sizes of 20 and 85 nm (solution of **4-K**) and 25 and 98 nm (solution of **5-K**). The characteristic DLS profiles of **4-K** and **5-K** aqueous solutions are shown in Fig. 2. Some large particles (*ca.* 10^5 nm in size) observed in the samples in small amounts (3–5%) are formed, most probably, *via* aggregation of many smaller nanostructures (*e.g.* 85–100 nm in size) into micrometer-sized clusters.

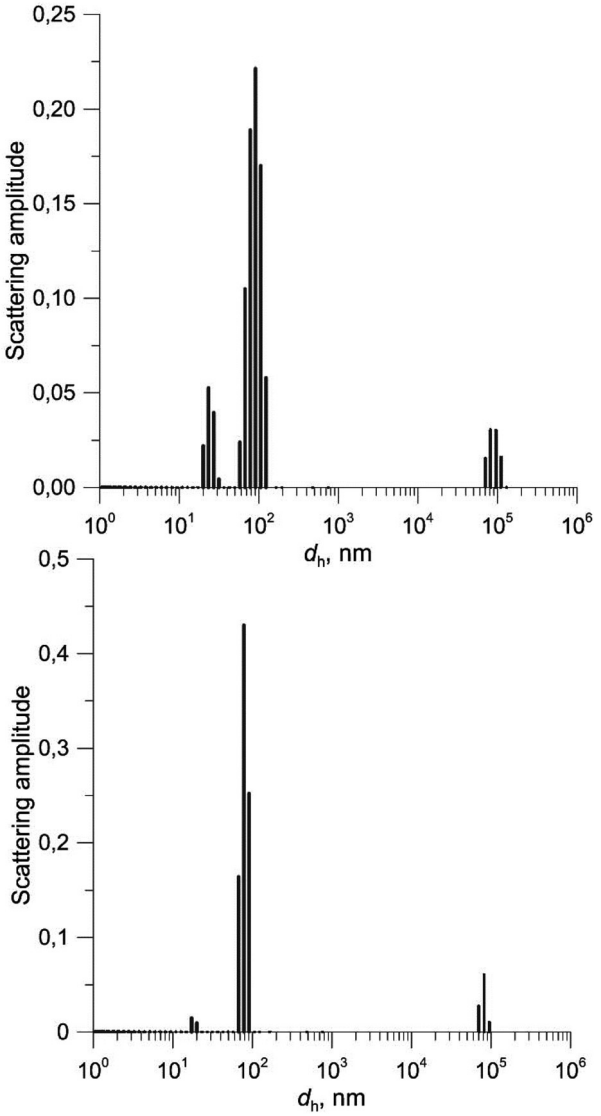

Fig. 2 DLS profiles of aqueous solutions of **4-K** (a) and **5-K** (b).

3.2. Photophysical properties of 4 and 5

The absorption spectrum of ruboxyl was shown to be very similar to that of doxorubicin in the visible range. However, ruboxyl shows stronger absorptions in the UV range at $\lambda < 350$ nm which can be explained by the contribution of the nitroxyl moiety to the absorption (Fig. 3).

It is known that daunorubicin or doxorubicin (daunorubicin analog) have rather intensive absorption bands in the visible spectral range with λ_{max} = 480–500 nm (ε_{485} = 11.5 × 10^3 M^{-1} cm^{-1} [29]). At the same time they show intense fluorescence with a band maximum at 590 nm.[30]

It has been shown also that ruboxyl demonstrates rather intense photoluminescence. The shape and the position of the photoluminescence band of ruboxyl resembles closely the fluorescence spectrum of doxorubicin (Fig. 4). The absorption spectra of hybrid nanostructures **4** and **5** are represented by the superpositions of the absorptions of individual fullerene derivatives and ruboxyl. The absorption profiles of the ruboxyl and the fullerene units remain almost unchanged contributing equally to the resulting absorption spectra of **4** and **5** (Fig. 3).

A comparative analysis of the luminescence parameters of individual ruboxyl **3** and fullerene–ruboxyl conjugates evidences perfect fluorescence quenching of ruboxyl by the

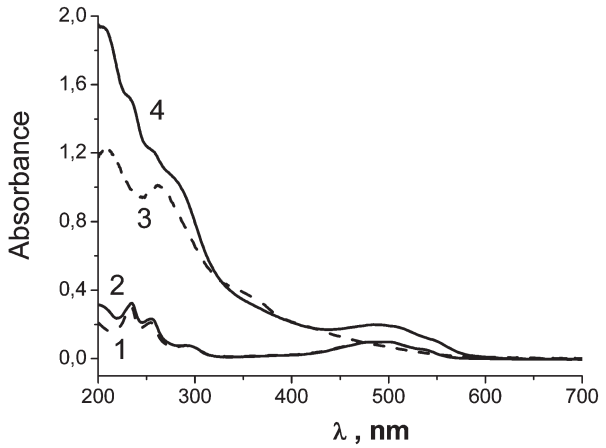

Fig. 3 Absorption spectra of doxorubicin (1), ruboxyl (2), compound **2** (3) and compound **4** (4) at a concentration of 10^{-5} M in phosphate buffer (pH = 6.5, 0.05 M).

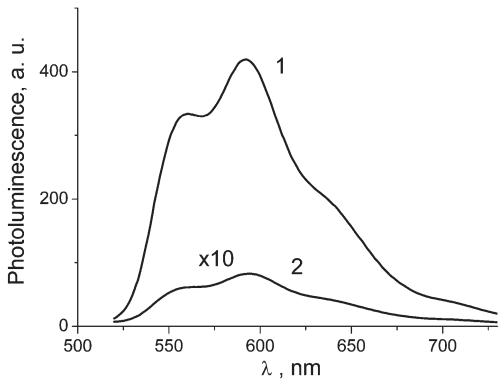

Fig. 4 Photoluminescence spectra of ruboxyl (line 1) and compound **4** (multiplied by 10) (line 2) at a concentration of 10^{-6} M in phosphate buffer (pH = 6.5, 0.05 M). λ_{ex} = 490 nm.

fullerene core in **4** and **5**. The fluorescence intensity of the hybrid nanostructures **4** and **5** amounts to 2% of the fluorescence intensity of pristine ruboxyl (Fig. 5). At the same time the fluorescence decay curves of these samples are monoexponential and have the same decay times as pristine ruboxyl (1.0 ns) (Fig. 5). This fact could be explained by a strong (or even complete) quenching of the ruboxyl unit fluorescence in nanostructures **4** and **5** by the fullerene core (more than 100 times). The observed residual weak fluorescence could be attributed to the 1–2% impurity of pristine ruboxyl in the samples of HNS **4** and **5**.

Considering the spectral and electronic properties of the investigated systems one could propose two mechanisms for the fluorescence quenching in the fullerene–ruboxyl nanostructures which are Förster energy transfer and photoinduced electron transfer.

It is known that the Förster energy transfer is realized when the luminescence spectrum of a donor (ruboxyl) overlaps considerably with the absorption spectrum of the acceptor (fullerene). Indeed, some such overlapping can be noticed in the case of ruboxyl–fullerene systems (Fig. 3 and 4), though the

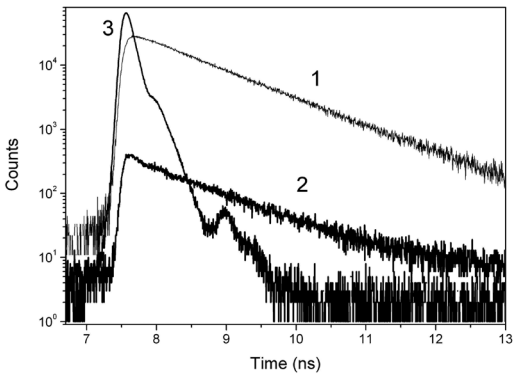

Fig. 5 Fluorescence decay profiles for 10^{-6} M solutions of ruboxyl (1) and compound **4** (2) in phosphate buffer (pH = 6.5, 0.05 M). λ_{ex} = 470 nm, λ_{em} = 590 nm. The instrument response function is also shown (3).

intensity of the fullerene absorptions in the 450–700 nm range is rather weak.

Assuming dipole–dipole excitation energy transfer, according to the Förster theory,[31] the following equation can be used to calculate R_0, which is a characteristic distance between the donor and the acceptor units, providing fluorescence quenching by 50%:

$$R_0{}^6 = \frac{9000 \ln 10 \times k^2 Q_d}{128 \pi^5 n^4 N} \int_0^\infty f_s(\nu) \times \varepsilon_A(\nu) \times \frac{d\nu}{\nu^4} \qquad (1)$$

the Q_d in eqn (1) is the quantum yield of the donor fluorescence, n is the refractive index of the solvent, N is the Avogadro constant, ε_A is the molar extinction of the energy acceptor A, $f_S(\nu)$ is the luminescence normalized spectrum, and k is an orientation factor. It is known that k^2 = 2/3 for systems with disordered orientations of the dipole moments of the transition.

Assuming that the efficiency of the fluorescence quenching due to the excitation energy transfer from the donor to the acceptor units is expressed by the I_0/I ratio, where I_0 and I are the intensities of the donor fluorescence in the absence and in the presence of the acceptor, respectively, one can determine the characteristic distance R between the donor and acceptor using the eqn (2).

$$R = \frac{R_0}{\sqrt[6]{\frac{I_0}{I} - 1}} \qquad (2)$$

the R_0 value of 22.7 Å can be calculated for the ruboxyl–fullerene conjugate using eqn (1), Q_d = 0.05[32] and n = 1.33. The ruboxyl fluorescence quenching factors $I_0/I > 100$ were experimentally obtained for the conjugates **4** and **5**. Using these quenching factors, eqn (2) and the R_0 value obtained from eqn (1) allowed us to estimate the characteristic distances between the chromophore (anthracycline part of ruboxyl) and the fullerene cage. These distances were found to be <10.6 Å for **4** and **5**. A simple estimation using 3D molecular models of **4** and **5** has shown that such distances between the

anthracycline fragment of ruboxyl and the fullerene core could be realized in hybrid structures of **4** and **5** due to the twisted conformation of the connected chain of chemical bonds. The observed reasonably good agreement between the R values obtained from the experimental data using Förster theory and the possible chromophore–fullerene distances derived from the chemical structures of **4** and **5** suggests that the Förster energy transfer can contribute to the photoluminescence quenching in these systems.

Alternatively, the ruboxyl fluorescence can be quenched *via* the electron transfer pathway from the ruboxyl excited state to the fullerene core. According to the common theory, the efficiency of the electron transfer from the donor to the acceptor molecules depends exponentially on the transfer distance R, free activation energy ΔG and the reorganization energy λ.[33,34] Under the optimal reaction conditions the electron transfer rate can be estimated using the following equation:

$$k_{et}^{NA} = k_0 \exp(-\alpha R), \quad (3)$$

This equation was empirically derived by an extensive analysis of the data on the electron transfer in various molecular architectures including photoactivated donor–acceptor systems.[35–38] According to the cited reports the k_0 in eqn (3) is equal to 10^{16} s^{-1}, R is the distance between the edge atoms of transfer centers, α is a parameter which accounts for the effect of the medium on the overlapping of the donor and acceptor wave functions *via* the superexchange interactions. Depending on the medium properties (intermolecular transfer) or the structure of the spacer (intramolecular transfer) separating the donor and acceptor moieties (*e.g.* saturated hydrocarbon chain, polypeptide chains possessing different superstructures, organic solvent, water or vacuum), the α parameter varies quite significantly. For example, α is close to 0.9 A^{-1} for saturated hydrocarbon chains, 1.4 A^{-1} for protein globules and 1.8–2.4 A^{-1} for water molecules.[39]

Considering the lifetime of the ruboxyl excited state of 1.0 ns (Fig. 5) (close to 1.1 ns for daunorubicin according to ref. 30) and the fluorescence quenching factor of >100, one can estimate a value of $k_{et} > 10^{11}$ s^{-1}. The electron transfer distances R of <8–13 Å could be estimated for the conjugates **4** and **5** using eqn (3) with α = 0.9–1.4 A^{-1}. These distances look very realistic for certain conformations of the spacers linking the ruboxyl and the fullerene moieties in **4** and **5**.

Thus, the analysis of the ruboxyl photoluminescence quenching in the hybrid nanostructures **4** and **5** suggests two possible pathways operating *via* energy transfer or photoinduced electron transfer from the ruboxyl unit to the fullerene core. The obtained experimental data do not allow one to make an unambiguous conclusion about relative contributions of each pathway to the ruboxyl photoluminescence quenching in **4** and **5**. Regardless of the operating mechanisms, the ruboxyl attached to the fullerene cage serves as a photosensitizer allowing for the efficient generation of the fullerene active species (fullerene excited states or fullerene radical anion) under visible light irradiation conditions. The following reactions of the photoexcited fullerene–ruboxyl nanostructures with molecular oxygen are expected to produce some active oxygen species such as singlet oxygen and superoxide radical anion, which is a key event in the photodynamic therapy.

3.3. Photodynamic properties of 4 and 5

Photochemical activity of the fullerene derivatives **1** and **2**, ruboxyl **3** and the hybrid nanostructures **4** and **5** was investigated by exciting the samples with visible and UV light. The excitation of the ruboxyl block has been performed using visible light matching well its absorption band with λ_{max} = 500 nm (Fig. 3). The fullerene core was excited using UV light with λ_{max} = 360 nm. The formation of the superoxide radical anions $O_2^{\cdot -}$ in our experiments was monitored using the standard formazan essay. The reaction of $O_2^{\cdot -}$ with NBT (nitro blue tetrazolium chloride) produces formazan which has an intense absorption in the visible range with λ_{max} = 560 nm.

It was shown that the illumination of the aerated aqueous solutions of the fullerene derivatives **1** and **2** using both UV (λ_{max} = 360 nm) and visible (λ_{max} = 500 nm) excitation produces active oxygen species quite efficiently (Fig. 6) which agrees well with the results published previously for other types of fullerene derivatives. Ruboxyl **3**, on the contrary, showed no production of the active oxygen species under illumination with visible light (λ_{max} = 500 nm). The attachment of the ruboxyl chromophore to the fullerene derivatives enhances the rate of generation of the active oxygen species. Thus, an improvement by a factor of two was observed for conjugate **4**, while conjugate **5** showed more than three times higher active oxygen production rate compared to the precursor fullerene derivative **2**.

The observed improvement correlates well with the optical properties of the fullerene derivatives **1–2** and the hybrid

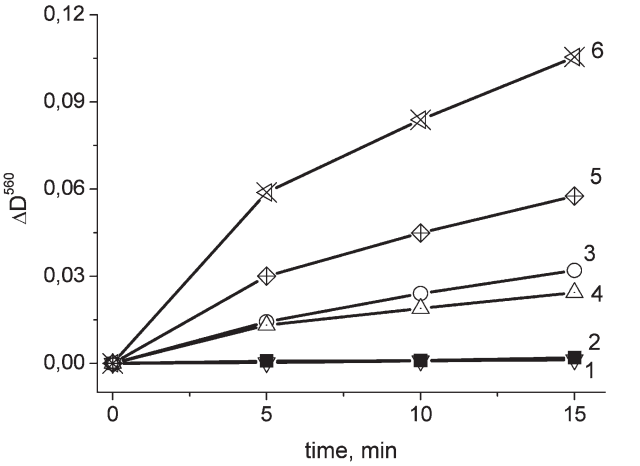

Fig. 6 Kinetics of $O_2^{\cdot -}$ formation under visible light irradiation (λ_{max} = 500 nm) using compounds **1–5** as sensitizers. The data points were obtained by monitoring the changes in the optical density ΔD_{560} of the solution at 560 nm (the formazan absorption band maximum) and plotted as a function of the irradiation time 1 – control (in the absence of **1–5**), 2 – sensitization with ruboxyl **3**, 3 – sensitization with compound **1**, 4 – sensitization with compound **2**, 5 – sensitization with conjugate **4**, 6 – sensitization with conjugate **5**.

nanostructures **4–5**. Indeed, the addition of the ruboxyl to the fullerene derivative increases the molar absorption by a factor of two in the 450–550 nm range due to the contribution of the anthracycline fragment. This result shows clearly that the ruboxyl moiety attached to the fullerene derivative works as a photoactivator improving the photodynamic properties of these hybrid nanoarchitectures.

4. Conclusions

A novel type of photoactive architecture has been successfully designed by conjugating the anticancer anthracycline antibiotic ruboxyl with water soluble fullerene derivatives. Dynamic light scattering experiments have shown that the synthesized conjugates undergo association in aqueous solutions with the formation of supramolecular nanostructures with characteristic hydrodynamic sizes of 85 and 98 nm. The photophysical properties and the photodynamic action of the ruboxyl–fullerene nanostructures were extensively investigated. It has been shown unambiguously that the anthracycline chromophore of the ruboxyl (having no photodynamic activity) behaves as an efficient photosensitizer for the fullerene core operating *via* energy and/or electron transfer pathways. The presented approach opens up wide opportunities for the design of various fullerene-based donor–acceptor systems with enhanced photodynamic properties potentially suitable for biomedicinal applications.

Acknowledgements

This work was supported by the RFBR (grants 10-03-00687 and 12-03-33031), the Russian President Science Foundation (MK-6177.2013.3) and the Presidium of Russian Academy of Sciences (Research program No 24 "Fundamental research in the field of nanotechnology and nanomaterials").

Notes and references

1 J. W. Aborgast, A. P. Darmanyan, C. S. Foote, F. N. Diederich, Y. Rubin, F. Diederich, M. M. Alvarez, S. J. Anz and R. L. Whetten, *J. Phys. Chem.*, 1991, **95**, 11–12.
2 Y. Yamakoshi, N. Umezawa, A. Ryu, K. Arakane, N. Miyata, Y. Goda, T. Masumizu and T. Nagano, *J. Am. Chem. Soc.*, 2003, **125**, 12803–12809.
3 B. Zhao, Yu.-Y. He, C. F. Chignell, J.-J. Yin and U. Andley, *Chem. Res. Toxicol.*, 2009, **22**, 660–667.
4 P. Mroz, A. Pawlak, M. Satti, H. Lee, T. Wharton, H. Gali, T. Sarna and M. R. Hamblin, *Free Radical Biol. Med.*, 2007, **43**, 711–719.
5 X. L. Yang, C. Huang, X. G. Qiao, L. Yao, D. X. Zhao and X. Tan, *Toxicol. in Vitro*, 2007, **21**, 1493–1498.
6 M. B. Spesia, M. E. Milanesio and E. N. Durantini, *Eur. J. Med. Chem.*, 2008, **43**, 853–861.
7 N. Nitta, A. Seko, A. Sonoda, S. Ohta, T. Tanaka, M. Takahashi, K. Murata, S. Takemura, T. Sakamoto and Y. Tabata, *CardioVasc. Interventional Radiol.*, 2008, **31**, 359–366.
8 Y. Doi, A. Ikeda, M. Akiyama, M. Nagano, T. Shigematsu, T. Ogawa, T. Takeya and T. Nagasaki, *Chem.–Eur. J.*, 2008, **14**, 8892–8897.
9 I. Lee, Y. Mackeyev, M. Cho, D. Li, J. H. Kim, L. J. Wilson and P. J. Alvarez, *Environ. Sci. Technol.*, 2009, **43**, 6604–6610.
10 L. Huang, M. Terakawa, T. Zhiyentayev, Y. Y. Huang, Y. Sawayama, A. Jahnke, G. P. Tegos, T. Wharton and M. R. Hamblin, *Nanomed.: Nanotechnol., Biol. Med.*, 2010, **6**, 442–452.
11 M. Hurtgen, A. Debuigne, A. Mouithys-Mickalad, R. Jérôme, C. Jérôme and C. Detrembleur, *Chem.–Asian J.*, 2010, **5**, 859–868.
12 J. Liu and Y. Tabata, *J. Drug Targeting*, 2010, **18**, 602–610.
13 E. Otake, S. Sakuma, K. Torii, A. Maeda, H. Ohi, S. Yano and A. Morita, *Photochem. Photobiol.*, 2010, **86**, 1356–1363.
14 Z. Lu, T. Dai, L. Huang, D. B. Kurup, G. P. Tegos, A. Jahnke, T. Wharton and M. R. Hamblin, *Nanomedicine*, 2010, **5**, 1525–1533.
15 R. Berera, G. F. Moore, I. H. M. Van Stokkum, G. Kodis, P. A. Liddell, M. Gervaldo, R. Van Grondelle, J. T. M. Kennis, D. Gust, T. A. Moore and A. I. Moore, *Photochem. Photobiol. Sci.*, 2006, **5**, 1142–1149.
16 F. D'Souza, P. M. Smith, M. E. Zandler, A. L. McCarty, M. Itou, Y. Araki and O. Ito, *J. Am. Chem. Soc.*, 2004, **126**, 7898–7907.
17 E. Maligaspe, N. V. Tkachenko, N. K. Subbaiyan, R. Chitta, M. E. Zandler, H. Lemmetyinen and F. D'Souza, *J. Phys. Chem. A*, 2009, **113**, 8478–8489.
18 D. Jarzab, F. Cordella, M. Lenes, F. B. Kooistra, P. W. M. Blom, J. C. Hummelen and M. A. Loi, *J. Phys. Chem. B*, 2009, **113**, 16513–16517.
19 D. Gust, T. A. Moore and A. L. Moore, *Acc. Chem. Res.*, 2009, **42**, 1890–1898.
20 M. Quintiliani, A. Kahnt, T. Wolfle, W. Hieringer, P. Vazquez, A. Gorling, D. M. Guldi and T. Torres, *Chem.–Eur. J.*, 2008, **14**, 3765–3775.
21 Y. N. Yamakoshi, T. Yagami, S. Sueyoshi and N. Miyata, *J. Org. Chem.*, 1996, **61**, 7236–7237.
22 M. E. Milanesio, M. G. Alvarez, V. Rivarola, J. J. Silber and E. N. Durantini, *Photochem. Photobiol.*, 2005, **81**, 891–897.
23 K. Okuda, Ch. Abeta, T. Hirota, M. Mochizuki and T. Mashino, *Chem. Pharm. Bull.*, 2002, **50**, 985–987.
24 C. Constantin, M. Neagu, R. M. Ion, M. Gherghiceanu and C. Stavaru, *Nanomedicine*, 2010, **5**, 307–317.
25 F. Franchi, N. P. Konovalova, P. Seminara, R. D. Diatchkovskaya, L. V. Volkova and L. Bonomo, *Cancer Ther. Control*, 1992, **2**, 199–205.
26 *RF Pat*, 2011111783, 2011.
27 O. Troshina, P. Troshin, A. Peregudov, V. Kozlovskiy, J. Balzarini and R. Lyubovskaya, *Org. Biomol. Chem.*, 2007, **5**, 2783–2791.

28 E. A. Khakina, A. A. Yurkova, A. A. Peregudov, S. I. Troyanov, V. Trush, A. I. Vovk, A. V. Mumyatov, V. M. Martynenko, J. Balzarini and P. A. Troshin, *Chem. Commun.*, 2012, **48**, 7158–7160.
29 L. Gallois, M. Fiallo, A. Laigle, W. Priebe and A. Garnier-Suillerot, *Eur. J. Biochem.*, 1996, **241**, 879–887.
30 M. Than Htun, *J. Lumin.*, 2009, **129**, 344–348.
31 Th. Förster, *Ann. Phys.*, 1948, **2**, 55–75.
32 J.-H. Liu, L. Cao, P. G. Luo, Sh-T. Yang, F. Lu, H. Wang, M. J. Meziani, S. A. Haque, Y. Liu, S. Lacher and Y.-P. Sun, *ACS Appl. Mater. Interfaces*, 2010, **2**, 1384–1389.
33 V. G. Levich and R. R. Dogonadze, *Dokl. Akad. Nauk*, 1959, **124**, 123.
34 R. A. Marcus and N. Sutin, *Biochim. Biophys. Acta, Rev. Bioenerg.*, 1985, **811**, 265–322.
35 A. I. Kotelnikov, *Biophysics*, 1993, **38**, 228–232.
36 C. C. Moser, J. M. Keske, K. Warncke, R. S. Farid and P. L. Dutton, *Nature*, 1992, **355**, 796–802.
37 A. I. Kotelnikov, V. R. Vogel, A. V. Pastuchov, V. L. Voskoboinikov and E. S. Medvedev, in *Biological electron-transfer chains: genetic, composition and mode of operation*, ed. G. W. Canters and E. Vijgenboom, Kluwer Academic Publishers, Dordrecht/Boston/London, 1998, vol. 512, pp. 27–50.
38 A. I. Kotelnikov, E. S. Medvedev and N. S. Goryachev, *Russ. Chem. Bull., Int. Ed.*, 2011, **60**, 1295–1318.
39 H. B. Gray and J. R. Winkler, in *The porphyrin handbook*, ed. K. M. Kadish, K. M. Smith and R. Guilard, Bioinorganic and Bioorganic Chemistry, Elsevier, Amsterdam, 2003, vol. 11, pp. 63–73.

